Analysis of characteristic prediction of aluminized boron steel after the hot stamping process using an image color-based neural network

Seung Chae Yoon (scyoon@hyundai-steel.com)
Hyundai Steel Co Ltd https://orcid.org/0000-0002-2027-3757
Je Youl Kong
Jea Myoung Park
Kye Jeong Park
Joo Sik Hyun

Research Article

Keywords: Hot stamping, Color difference, CIE-Lab, Neural network, Mechanical performance, Process conditions, Inter-diffusion layer, Hydrogen uptake

Posted Date: July 10th, 2023

DOI: https://doi.org/10.21203/rs.3.rs-3113162/v1

Version of Record: A version of this preprint was published at The International Journal of Advanced Manufacturing Technology on November 23rd, 2023. See the published version at https://doi.org/10.1007/s00170-023-12477-9.

Abstract

Hot stamping is an innovative technology that enables the production of high-strength automotive body parts by heating the material to a high temperature and simultaneously forming and quenching it in-die. The process results in parts with excellent strength-to-weight ratios, which are essential for the automotive industry. The widely used 22MnB5 material is heated to temperatures above 900°C, and an Al-Si coating is applied to prevent the formation of oxide scale on the sheet surface. The distinctive color on the sheet surface after hot stamping is produced by the Al-Si coating. This phenomenon is attributed to the formation of Al_2O_3 on the surface of the Al-Si coating layer and the diffusion of Fe from the substrate into the Al-Si coating layer, both of which are significantly influenced by the heating time and temperature. In this study, the neural network was investigated to predict the hot stamping heating temperature and time conditions based on the color exhibited on the sheet surface after the process. Additionally, the neural network was combined with numerical models to predict the inter-diffusion layer thickness in the Al-Si coating layer, which affects the weldability of the vehicle part, and the amount of hydrogen uptake that directly influences hydrogen embrittlement.

1. Introduction

Recently, the application ratio of high-strength steel over 1 GPa has increased to reduce the vehicle body weight and meet fuel efficiency regulations [1, 2]. In addition, it is necessary to maintain the stability of high-strength body parts of vehicles to meet strengthened crash requirements [3, 4]. This aims not only to reduce vehicle body weight but also to ensure the safety of passengers in the event of a crash [1–4]. Although the application ratio is increasing to maximize the effect of applying an advanced high-strength steel sheet to the vehicle body, it is difficult to freely apply it to various parts due to the forming limit and dimensional precision of high-strength sheet materials [5–10]. Hot stamping technology can easily address these challenges [5, 6]. This is because the 22MnB5 can be heated at high temperatures to ensure formability, and a strength of 1.5 GPa or more can be secured through in-die quenching [6–9]. In addition, the application of hot stamping materials and related technologies has increased to the extent that it serves their purpose in the transition to eco-friendly vehicles. This is because these technologies are very effective not only in protecting passengers during a crash but also in achieving additional weight reduction as weight increases due to increased battery capacity for long-distance driving and enhanced functions that can prevent battery explosions [8, 9]. However, the above techniques have challenges in the application of some engineering solutions such as deformation, heat properties, and phase transformation at temperatures of 900 ℃ or higher; thus, a significant amount of material information is required in advance. Furthermore, existing research has difficulty capturing material behavior under hot stamping conditions [5–12].

In the hot stamping process, a few coatings have been used to prevent oxide scale formation on the sheet surface during austenitization in the furnace, with Al-Si coating being the most common protection [12, 13]. For Al-Si coating, the remaining phases vary in proportion to the target temperature, and the coated layer structure can be controlled by analyzing the phase growth mechanism in Al-Si coated layers [13].

After the austenite transformation temperature, the existing Al-Si coated layer structure is altered at the target temperature, resulting in the formation of different cracks and voids in the Al-Si coated layer.

As shown in Fig. 1, the difference in surface color is due to light diffraction caused by the Al_2O_3 oxide film and the diffusion of the Fe substrate into the Al-Si coated layer [13]. The Al-Si coated surface has an individual color that occurred at high temperatures depending on the heating conditions in the manufacturing field. This individual color can occasionally provide information about hot stamping product performance in terms of weldability and hydrogen embrittlement. For example, the performance has been deemed negative in cases of reddish-yellow color based on the individual colors of hot stamping parts. This could be due to the phenomena of thickening inter-diffusion layers and an increased number of voids that occur when the heating time and temperature exceed the standard; moreover, it is difficult to objectively analyze the degree of color difference by visibility. Furthermore, the reliability of such analysis is insufficient because the quality level is determined visually in comparison to other parts that have a distinctive color difference.

Therefore, this study aims to objectify the color differences of hot stamping parts, spanning from bluish to reddish hues, which were previously challenging to distinguish by human vision. To achieve this, a machine learning (ML) approach using a neural network (NN) has been adopted. Additionally, essential process information for predicting hot stamping performance was analyzed using the color difference system.

2. Analysis of the prediction of individual color differences based on neural networks

Neural networks (NN), a subset of artificial intelligence, are extensively applied for addressing classification and regression challenges across multiple domains. Key research areas in NN encompass architecture and parameter search [14, 15]. Within convolutional neural networks (CNN), backpropagation, a parameter search method, is crucial, exhibiting exceptional performance in fields like natural language processing, computer vision, and speech recognition [14–20]. CNNs are structured with fully connected layers and employ a multi-layered neural network that includes an input layer, hidden layers, and an output layer [14–18]. The input layer accepts raw data, and the output layer delivers the results, while the intermediate layers act as hidden layers [17, 18]. Determining the optimal number of nodes for the hidden layer is a challenging task, with an increase in nodes leading to a higher computational complexity [18]. Conversely, a smaller node count in the hidden layer may diminish learning capability [18, 19]. The number of hidden nodes, represented by γ, can be calculated using the following equation:

$$\gamma = (\alpha + \beta)^{1/2} + l \quad \text{Eq. (1)}$$

Here, α signifies the number of input nodes, β the number of output nodes, and l is a constant ranging from 1 to 10 [18]. The total number of nodes in a fully connected NN can be computed as:

$$\mathcal{N} = \alpha + \gamma + \beta \quad \text{Eq. (2)}$$

In this formula, N denotes the total number of nodes. The total number of weights and thresholds requiring optimization can be determined as [18]:

$H = \gamma (\alpha + \beta) + \gamma + \beta$ Eq. (3)

In this equation, H denotes the total count of weights and thresholds that require optimization. The number of thresholds in the hidden layer is represented by γ, while β indicates the number of thresholds in the output layer [18]. To address problems that are intractable with a linear model, an activation function is employed to introduce non-linear factors [14–18]. This method enabled the implementation of an algorithm for analyzing color differences in hot stamping, facilitating the collection of consistent, objective information following the hot stamping process, devoid of human visual bias. To evaluate the generalizability of the newly trained NN, a set of test data, which was not part of the training phase, was inputted [19, 20]. This process is crucial to ensure that the NN can reliably predict outputs for new inputs if the discrepancy between the predicted and expected output values is sufficiently minimal, as shown in Fig. 2 [18–20].

In this study, the color change mechanism during the heating process of the Al-Si coating layer and the prediction of the hot stamping performance characteristics were analyzed. The color of the hot stamping part was analyzed using the ML algorithm with individual color difference data sets obtained from experiments. The initial input nodes were constructed by classifying the hot stamping color image into specific feature pixel sizes and rows. The NN was trained using segmented row data to learn the color information of the hot stamping part, as represented in Fig. 3. The backpropagation method was utilized to predict the heating temperature and time of the hot stamping Al-Si coating layer based on the specific color, and the obtained results were used to examine the technique of numerically deriving the inter-diffusion layer thickness and hydrogen uptake of the hot stamping Al-Si coating layer.

3. Results and discussion

As mentioned earlier, when Al-Si coated hot stamping material (22MnB5) is heated above the Ac3 temperature, the specific color appears due to the formation of Al_2O_3 film and diffusion into the Al-Si coating layer of Fe in the material [12, 13]. Figure 4 represents the surface colors of the hot stamping material under various heating conditions ranging from 860 ℃ to 950 ℃ and 180 to 600 seconds by CIE-Lab. It is defined by the International Commission on Illumination (CIE) and consists of three coordinates: L^*, a^*, and b^*. The L^* coordinate represents the lightness of the color, where $L^* = 0$ represents black and $L^* = 100$ represents white [21]. The a^* coordinate represents the color's position between red and green, with positive values indicating red and negative values indicating green [20, 21]. The b^* coordinate represents the color's position between yellow and blue, with positive values indicating yellow and negative values indicating blue. The color difference will primarily be explained based on the a^* and b^* coordinates [13, 21]

As shown in Fig. 4, it can be observed that the color of the sheet changes towards reddish as the heating temperature and time increase. To analyze colors, it was generally intended to represent them as 2-dimensional arrays or matrices, with each component representing the point values of the data. The related mathematical expression can be represented as follows: If *X* is a dataset consisting of *p* data points and *q* dimensions; *X* can be represented as a p × q matrix [21].

$$X = \begin{bmatrix} x_{11} & \cdots & x_{1q} \\ \vdots & \ddots & \vdots \\ x_{p1} & \cdots & x_{pq} \end{bmatrix} \quad \text{Eq. (4)}$$

Each data point x_{ij} is represented by a color, and its value is determined by normalization and the color itself. In other words, the value of the data point x_{ij} can be normalized using the following formula [18–21]:

$$\widehat{x_{i,j}} = \frac{x_{ij} - min(X)}{man(X) - min(X)} \quad \text{Eq. (5)}$$

Where, *min(X)* represents the minimum value of *X*, *max(X)* represents the maximum value of *X*, and $\widehat{x_{i,j}}$ is the normalized value of x_{ij}. Each data point x_{ij} can be indicated as the color in the following method [18–21].

$$color\left(x_{i,j}\right) = C(\widehat{x_{i,j}}) \quad \text{Eq. (6)}$$

The $color(x_{i,j})$ represents the color corresponding to x_{ij}, and this color representation allows for visualization through data point values [18–21]. The colors resulting from variations in hot stamping heating temperature and time were represented as a CIE-Lab based color map. Figure 5 (a) shows the color changes obtained from experiments conducted at heating times of 180 to 600 seconds and the heating temperature of 950 ℃, represented by the intensity of CIE-Lab. It can be observed that as the heating time increases, the *a** coordinate of CIE-Lab moves from negative to positive values, while the *b** coordinate changes from negative to positive values. The *L** coordinate indicates the distribution of 35 ~ 44. Figure 5 (b) represents the color changes observed in experiments conducted at the heating time of 300 seconds and heating temperatures ranging from 860 to 950 ℃, represented by the intensity of CIE-Lab. It is noticed that the trend with increasing temperature is quite different from that observed with varying heating times. As the temperature increases, the *a** coordinate changes from positive to negative, while the *b** coordinate changes from positive to negative as well. The *L** coordinate is observed to have a distribution of 35 ~ 44. These relationships are expressed using Eq. (6); and each *L*a*b** coordinate is quantified according to the heating temperature and time, as seen in Fig. 6. It is observed that the *L** and *a** coordinates mainly react to changes in the heating temperature, while the *L** and *b** coordinates are mainly affected by changes in the heating time. However, it can be observed that the *a** coordinate is mainly affected by the heating temperature and the *b** coordinate is mainly affected by the heating time when excluding the *L** coordinate, which has a similar variation range obtained from the experimental results.

Based on the color difference by CIE-Lab, the aim was to predict the heating temperature and time, as well as the inter-diffusion layer thickness that affects weldability and hydrogen uptake that affects hydrogen embrittlement, using the color of the part image and the training algorithm.

1) Analysis of color difference by hot stamping conditions

To evaluate the surface color of hot stamping sheets, which have undergone the specific manufacturing process, the colorimeter, and the NN model were utilized, and their results were compared. CIE-Lab standard was employed to analyze the color of the hot stamping sheets, resulting in the average NN model and colorimeter results being found to be similar. Based on this, the NN model was used to predict the hot stamping heating conditions of 880 ℃ for 300 seconds for (a), 930 ℃ for 300 seconds for (b), and 960 ℃ for 300 seconds for (c), as represented in Fig. 7. To validate this consistency across a wider range, the results were analyzed in the CIE-Lab range of -10 to + 10. As shown in Fig. 8, it was confirmed that the statistical R^2 trend between the obtained colors and the predicted values by the NN model was about 0.99 or higher. While the colorimeter has the disadvantage of only analyzing the color in the limited local area, making real-time analysis difficult, the NN model has the advantage of being able to analyze a wide range of colors in real-time using only image information. By integrating this image-based color analysis technology with hot stamping manufacturing technology, it is expected that hot stamping manufacturing monitoring and real-time analysis can be performed.

2) Inter-diffusion layer thickness prediction using color analysis

Evaluation of resistance spot welding characteristics has to be performed for the application of hot stamping vehicle parts. The Al-Si coated 22MnB5 material changes the coating layer depending on the heating temperature and time; typically there were 4 layers in the Al-Si coating [22]. In particular, the inter-diffusion layer is formed at the boundary between the Al-Si coating and the Fe substrate, and it is known that it is advantageous for resistance spot welding to have a thickness of 15 μm or less [22, 23]. Also, depending on the heating conditions, voids are created and grown inside the inter-diffusion layer and on the surface of the coating layer, which increases resistance and affects spot welding characteristics [22–24]. Figure 9 shows optical microscopy analysis of cross-sections of coating layers after 300 seconds and 600 seconds at the heating condition of 950 ℃; (a) is after 300 seconds and (b) is after 600 seconds. In the cross-section heated for 300 seconds, the inter-diffusion layer of about 11.3 μm was formed, while in the cross-section heated for 600 seconds, the thickness of the inter-diffusion layer was about 19.15 μm and many voids were created on the surface.

As heating time increases, the thickness of the inter-diffusion layer increases, and voids increase, resulting in the deterioration of resistance spot welding characteristics [22]. To predict the inter-diffusion layer thickness that affects resistance spot welding characteristics, the present study aims to verify the FeAl intermetallic formation model [23, 24]. To predict the inter-diffusion layer thickness, the diffusion

principle of phase transformation in solids was considered to predict the overall coating thickness and the thickness of each layer of the coating generated by each phase [23].

$$IDY = G\sqrt{t} \quad \text{Eq. (7)}$$

In this Eq. (7), *IDY* denotes the layer thickness, *t* represents the soaking time, and *G* stands for the growth rate in units of μm/s^2. It is also noteworthy that the growth rate, *G*, can be described by $G = G_0 exp(-Q/RT)$, where G_0 is a constant, *Q* is the apparent activation energy, *T* is the soaking temperature measured in Kelvin, and *R* is the gas constant [23]. Furthermore, because the inter-diffusion layer comprises α-Fe and FeAl intermetallic, the model considering the properties of each phase is necessary [23, 24].

$$IDY = \left[G_{\alpha-Fe} exp\left(\frac{Q_{\alpha-Fe}}{RT}\right) + G_{FeAl} exp\left(\frac{Q_{FeAl}}{RT}\right)\right]\sqrt{t} \quad \text{Eq. (8)}$$

The values were calculated using $Q_{\alpha\text{-}Fe}$ of 182 KJ/mol and Q_{FeAl} of 250 KJ/mol [23], and the required temperature *(T)* and time *(t)* were determined by applying the results obtained from image analysis based on the NN model. To predict the inter-diffusion layer based on the aforementioned models, the center pillar component with the initial Al-Si coating weight of approximately 85 g/m^2 was used, as represented in Fig. 10.

The flat surface color was analyzed with the NN model, which predicted CIE-Lab values of -0.76 for *a** coordinate and − 7.75 for *b** coordinate, allowing for the prediction of the heating temperature of 970 °C and the time of 260 seconds. This was consistent with the real hot stamping heating conditions. Furthermore, applying the obtained temperature *(T)* and time *(t)* to Eq. (8) allowed for the inter-diffusion layer thickness analytical, which was predicted to be approximately 11.3 μm. This was found to be similar to the experimental thickness of the inter-diffusion layer obtained from the vehicle part, which was 11.8 μm, as shown in Fig. 11. The models and approach presented suggest that it is possible to predict the inter-diffusion layer thickness that affects the resistance spot welding characteristics using only image color analysis without specimen extraction.

3) Hydrogen uptake prediction by using color analysis

The Al-Si coated 22MnB5 material may undergo a process of brittleness due to the absorption of hydrogen when it is heated to achieve a higher strength [23–25]. The reason behind this is the diffusion of hydrogen into the austenite microstructure during the heating phase [24, 25]. After the phase transformation, the hydrogen is temporarily held within the internal microstructure, unable to exit through the Al-Si surface coating at room temperature until a sudden fracture takes place under residual or additional stress [25–29]. To avert the issue of hydrogen embrittlement, it is critical either to avert the absorption of hydrogen or to integrate processes that will eliminate the absorbed hydrogen [25]. In order to study these characteristics beforehand, the absorption of hydrogen was anticipated using the neural network-based image color analysis [24–27].

To predict hydrogen absorption, the well-known constant surface concentration diffusion model can be adopted [24]. This model can be used to analyze one-dimensional diffusion. Assuming that hydrogen is available for diffusion within the furnace, it is possible to calculate hydrogen absorption over time and distance [24–25].

$$\frac{C_s - C(x,t)}{C_s - C_0} = erf\left(\frac{x}{2\sqrt{Dt}}\right) \quad \text{Eq. (9)}$$

Here, C_0 represents the initial constant hydrogen concentration, x denotes the distance from the source of hydrogen, T is the heating temperature and t is the heating time [24–26]. In this case, the heating time is assumed as 1/3 of the total heating time, as the time spent at the austenite phase is significant. The diffusion coefficient D is used ($D = D_0 exp(-W/RT)$, where D_0 is 4.4×10^{-7} m/s^2, W is the apparent activation energy of 37 KJ/mol) at high temperatures [26–35]. Additionally, taking into account that hydrogen diffuses for both sides of the 22MnB5 sheet, x is set to half of the sheet thickness, which is 1.6mm. The temperature (T) and time (t) required for Eq. (9) was obtained from the color distribution in Fig. 10, as mentioned earlier. To analyze the diffusible hydrogen, the model validation was evaluated using the thermal desorption analysis (TDA) analysis [31, 32]. TDA analysis was conducted by heating the sheet at approximately 20 °C/min in the nitrogen atmosphere and analyzing the hydrogen desorption from the sheet in ppm/s units [31–35]. Figure 12 represents the hydrogen uptake of approximately 0.47 ppm based on the experimental center pillar vehicle part. With utilizing the diffusion model assuming the surface concentration within the heating process, it was determined that the value was approximately 0.58 ppm by using the diffusion model. These approach methods can also be achieved using extended constitutive models, such as hydrogen-assisted damage and others [31–33].

By employing the NN-based image color analysis, it was possible to predict the hot stamping heating temperature and time using only the color information obtained from vehicle part images, and its accuracy was considered to be high. In future work, hot stamping part performance will be investigated using finite element analysis in conjunction with constitutive models.

4. Conclusions

In this study, the main objective was to predict the heating temperature and time conditions and analyze the factors that influence the performance of vehicle parts by examining the surface color generated after the hot stamping process. To accomplish this, the image-based neural network was employed to obtain information on the heating temperature and time of hot stamping. The neural network's predictions enabled the estimation of the inter-diffusion layer thickness in the Al-Si coating layer and the hydrogen uptake in the hot stamping part. Gaining insights into these factors allows for the optimization of the hot stamping process, which in turn leads to improved performance and durability of the vehicle. The application of an image-based neural network in this study demonstrates the solution of machine learning in the field of materials science and manufacturing processes.

1) The neural network model was constructed using the dataset of color changes according to heating temperature and time by CIE-Lab coordinate. It was found to exhibit a similar trend compared to the conventional colorimeter. The statistical R^2 value was confirmed to be approximately 0.99 or higher.

2) By using the trained neural network model, it was possible to predict the heating temperature of 970 ℃ and time of 260 seconds obtained from the hot stamping color of the vehicle part, and it was confirmed to be consistent with the experimental conditions.

3) Through image analysis based on the NN model, the inter-diffusion layer thickness that affects the resistance spot weldability was predicted using the heating temperature and time obtained from image information. By considering the diffusion principle of phase transformation in solids, the value of approximately 11.3 μm was predicted, which was confirmed to be similar to the vehicle part analysis of 11.8 μm.

4) To predict the hydrogen uptake that affects the hot stamping hydrogen embrittlement, the constant surface concentration diffusion model was applied under basic assumptions. The results obtained from thermal desorption analysis were approximately 0.47 ppm, and the value predicted by reflecting the heating temperature and time obtained through image analysis based on the NN was confirmed to be approximately 0.58 ppm.

5) It was possible to predict the factors affecting weldability and hydrogen embrittlement with only image information, without destructive analysis of materials, by using color analysis based on the NN model to represent hot stamping heating temperature and time. This approach is considered a smart manufacturing solution that enables real-time performance analysis by linking with monitoring of the hot stamping manufacturing process.

Declarations

Authors contribution

Seung Chae Yoon: Writing original draft, Methodology. **Je Youl Kong:** Methodology, Investigation. **Jea Myoung Park:** Formal analysis, Data curation. **Kye Jeong Park:** Investigation, Formal analysis. **Joo Sik Hyun:** Supervision. All authors discussed the results and commented on the manuscript.

Conflict of Interest: The authors have no relevant financial or non-financial interests to disclose.

References

1. Hino R, Goto Y, Yoshida F (2003) Springback of sheet metal laminates in draw-bending. J Mater Process Technol 139:341–347. doi: 10.1016/s0924-0136(03)00541-7
2. Kim K-J, Han C-P, Lim J-H, et al (2012) Light-weight design and simulation of automotive rear bumper impact beam using boron steels. Trans Kor Soc Auto Eng 20:98–102. doi:

10.7467/ksae.2012.20.2.098

3. Bok H-H, Lee M-G, Kim H-D, Moon M-B (2010) Thermo-mechanical finite element analysis incorporating the temperature dependent stress-strain response of low alloy steel for practical application to the hot stamped part. Met Mater Int 16:185–195. doi: 10.1007/s12540-010-0405-0
4. Ma BL, Wan M, Wu XD, et al (2017) Investigation on forming limit of Advanced High Strength Steels (AHSS) under hot stamping conditions. J Manuf Processes 30:320–327. doi: 10.1016/j.jmapro.2017.10.001
5. Yoon SC, Kim DH (2013) Analysis of phase transformation and temperature history during hot stamping using the finite element method. Trans Mater Process 22:123–132. doi: 10.5228/kstp.2013.22.3.123
6. Xing ZW, Bao J, Yang YY (2009) Numerical simulation of hot stamping of quenchable boron steel. Mater Sci Eng A 499:28–31. doi: 10.1016/j.msea.2007.09.102
7. Kim HY, Park JK, Lee M-G (2013) Phase transformation-based finite element modeling to predict strength and deformation of press-hardened tubular automotive part. Int J Adv Manuf Technol 70:1787–1801. doi: 10.1007/s00170-013-5424-9
8. Min J, Lin J, Li J, Bao W (2010) Investigation on hot forming limits of high strength steel 22MnB5. Comput Mater Sci 49:326–332. doi: 10.1016/j.commatsci.2010.05.018
9. Cui J, Sun G, Xu J, et al (2015) A method to evaluate the formability of high-strength steel in hot stamping. Mater Des 77:95–109. doi: 10.1016/j.matdes.2015.04.009
10. Li FF, Fu MW, Lin JP (2015) Effect of cooling path on the phase transformation of Boron Steel 22MnB5 in hot stamping process. Int J Adv Manuf Technol 81:1391–1402. doi: 10.1007/s00170-015-7298-5
11. Banabic D (2005) An improved analytical description of orthotropy in metallic sheets. Int J Plast 21:493–512. doi: 10.1016/j.ijplas.2004.04.003
12. Merklein M, Lechler J (2008) Determination of material and process characteristics for hot stamping processes of quenchenable ultra high strength steels with respect to a Fe-based process design. SAE Int J Mater Manuf 1:411–426. doi: 10.4271/2008-01-0853
13. Yang W, Hwang E, Kim H, et al (2019) A study of annealing time to surface characteristics and hydrogen embrittlement on AlSi coated 22MnB5 during hot stamping process. Surf Coat Technol 378:124911. doi: 10.1016/j.surfcoat.2019.124911
14. Hornik K, Stinchcombe M, White H (1989) Multilayer feedforward networks are universal approximators. Neural Networks 2:359–366. doi: 10.1016/0893-6080(89)90020-8
15. Sejnowski TJ (1989) Neural network learning algorithms. Neural Computers 291–300. doi: 10.1007/978-3-642-83740-1_31
16. Larose DT, Larose CD (2014) Discovering knowledge in data: an introduction to data mining. John Wiley & Sons.

17. Guang-Bin Huang (2003) Learning capability and storage capacity of two-hidden-layer feedforward networks. IEEE Trans. Neural Networks 14:274–281. doi: 10.1109/tnn.2003.809401
18. Xue Y, Wang Y, Liang J (2022) A self-adaptive gradient descent search algorithm for fully-connected Neural Networks. Neurocomputing 478:70–80. doi: 10.1016/j.neucom.2022.01.001
19. Rumelhart DE, Hinton GE, Williams RJ (1986) Learning representations by back-propagating errors. Nature 323:533–536. doi: 10.1038/323533a0
20. Lin YC, Zhang J, Zhong J (2008) Application of neural networks to predict the elevated temperature flow behavior of a low alloy steel. Comput Mater Sci 43:752–758. doi: 10.1016/j.commatsci.2008.01.039
21. Chen Y, Zhang M, Fan D, et al (2018) Linear regression between CIE-lab color parameters and organic matter in soils of tea plantations. Eurasian Soil Sci 51:199–203. doi: 10.1134/s1064229318020011
22. US9708683B2 - coated steel strips, methods of making the same, methods of using the same, Stamping blanks prepared from the same, stamped products prepared from the same, and articles of manufacture which contain such a stamped product. In: Google Patents. https://patents.google.com/patent/US9708683/un.
23. Windmann M, Röttger A, Theisen W (2014) Formation of intermetallic phases in Al-coated hot-stamped 22MnB5 sheets in terms of coating thickness and Si content. Surf Coat Technol 246:17–25. doi: 10.1016/j.surfcoat.2014.02.056
24. Oldenburg M, Hardell J, Casellas D (2019) 7th International Conference Hot Sheet Metal Forming of high-performance steel, June 2-5, 2019, Luleå, Sweden proceedings. Verlag Wissenschaftliche Scripten, Auerbach/Vogtl.
25. Cho L, Sulistiyo DH, Seo EJ, et al (2018) Hydrogen absorption and embrittlement of ultra-high strength aluminized press hardening steel. Mater Sci Eng A 734:416–426. doi: 10.1016/j.msea.2018.08.003
26. Qiu C, Olson GB, Opalka SM, Anton DL (2004) Thermodynamic evaluation of the Al-H System. J Phase Equilib Diffus 25:520–527. doi: 10.1007/s11669-004-0065-1
27. Kiuchi K, McLellan RB (1983) The solubility and diffusivity of hydrogen in well-annealed and deformed iron. Acta Metall 31:961–984. doi: 10.1016/0001-6160(83)90192-x
28. Jakse N, Pasturel A (2014) The hydrogen diffusion in liquid aluminum alloys from *ab initio* molecular dynamics. J Chem Phys 141:094504. doi: 10.1063/1.4894225
29. Yakubtsov I, Sohmshetty R (2018) Evolution of Al-Si coating microstructure during heat-treatment of USIBOR®1500. IOP Conf Ser: Mater Sci Eng 418:012015. doi: 10.1088/1757-899x/418/1/012015
30. Itakura AN, Miyauchi N, Murase Y, et al (2021) Model of local hydrogen permeability in stainless steel with two coexisting structures. Sci Rep 11:8553. doi: 10.1038/s41598-021-87727-5
31. Xiukui S, Jian X, Yiyi L (1989) Hydrogen permeation behaviour in austenitic stainless steels. Mater Sci Eng A 114:179–187. doi: 10.1016/0921-5093(89)90857-5

32. Kumar P, Balasubramaniam R (1997) Determination of hydrogen diffusivity in austenitic stainless steels by subscale microhardness profiling. J Alloys Compd 255:130–134. doi: 10.1016/s0925-8388(96)02846-0
33. Liu Y, Chen Y, Yang C, Han X (2022) Study on hydrogen embrittlement and reversibility of hot-stamped aluminized 22MnB5 steel. Mater Sci Eng A 848:143411. doi: 10.1016/j.msea.2022.143411
34. Oriani RA (1970) The diffusion and trapping of hydrogen in Steel. Acta Metall 18:147–157. doi: 10.1016/0001-6160(70)90078-7
35. Kim H-J, Jung H-Y, Jung S-P, et al (2021) Hydrogen absorption and desorption behavior on aluminum-coated hot-stamped boron steel during hot press forming and automotive manufacturing processes. Materials 14:6730. doi: 10.3390/ma14216730

Figures

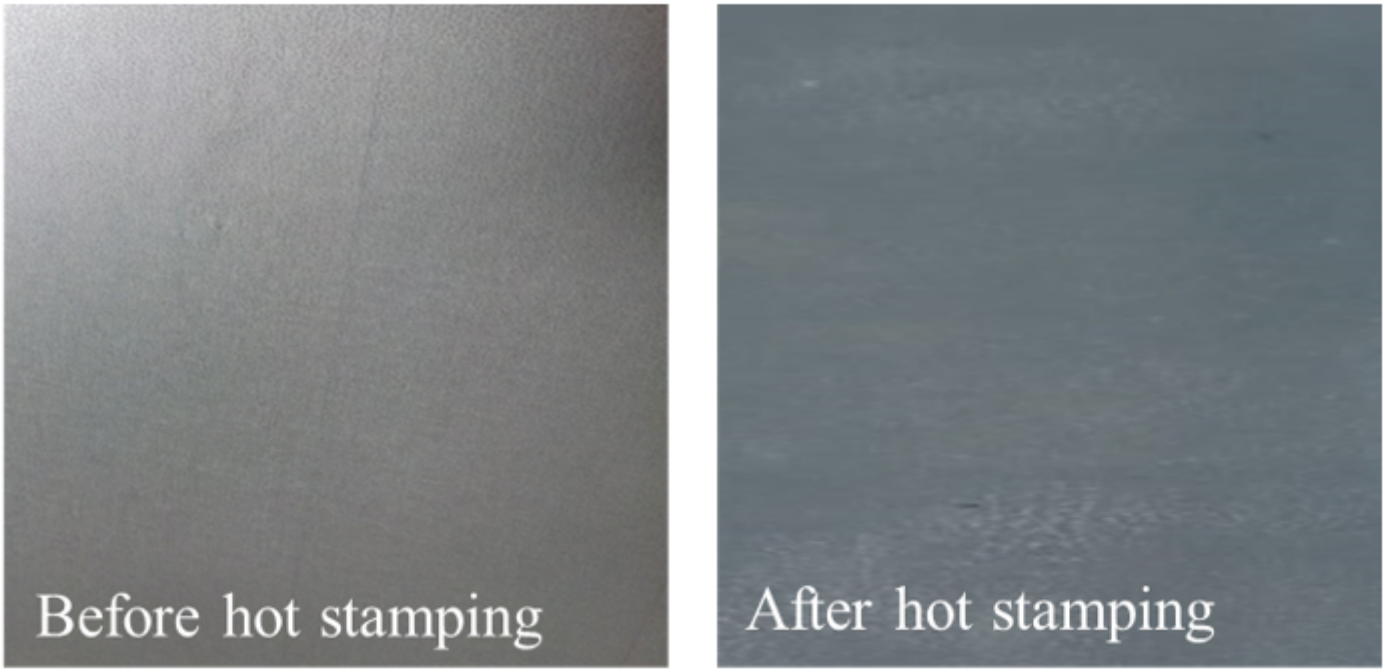

Figure 1

Comparison of hot stamping sheet color after the process.

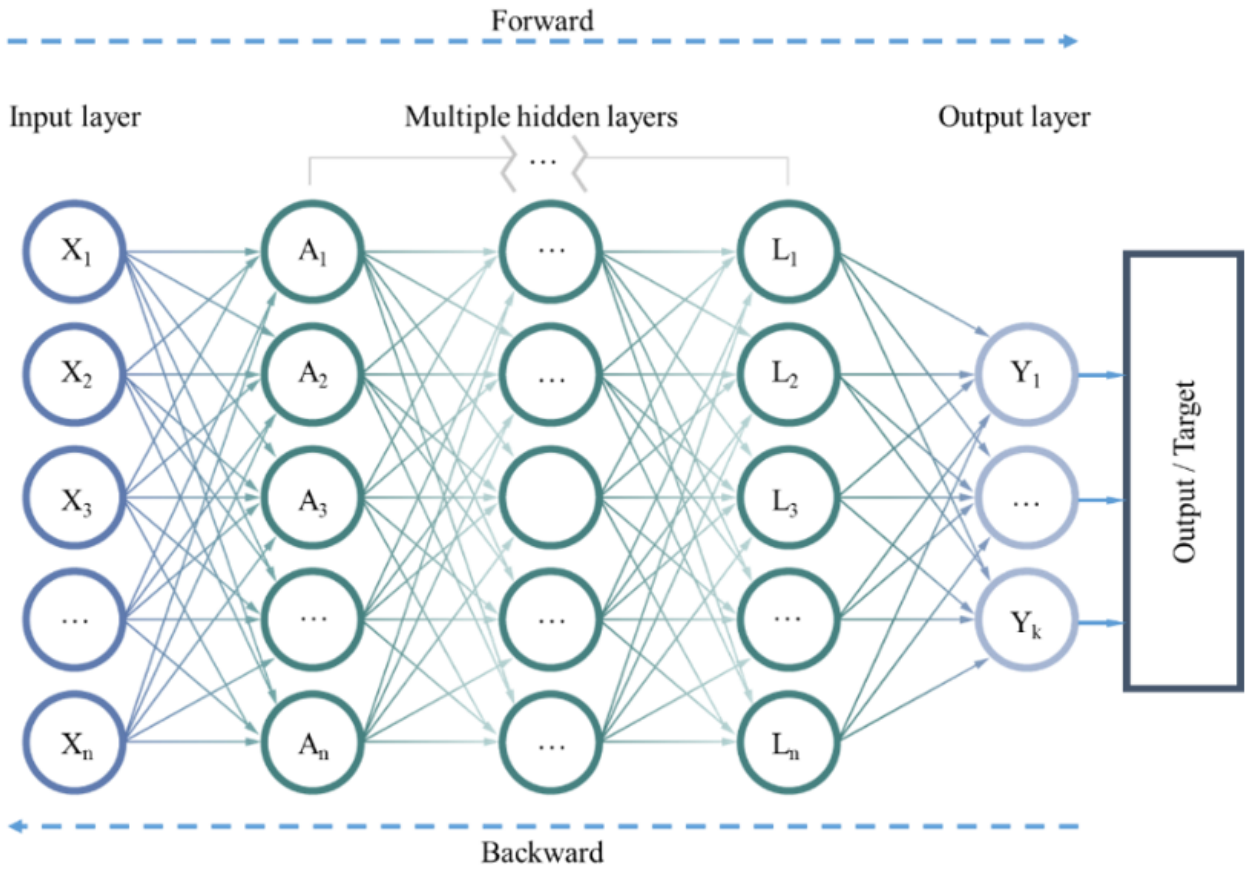

Figure 2

Schematic structure of back propagation neural network [18-20].

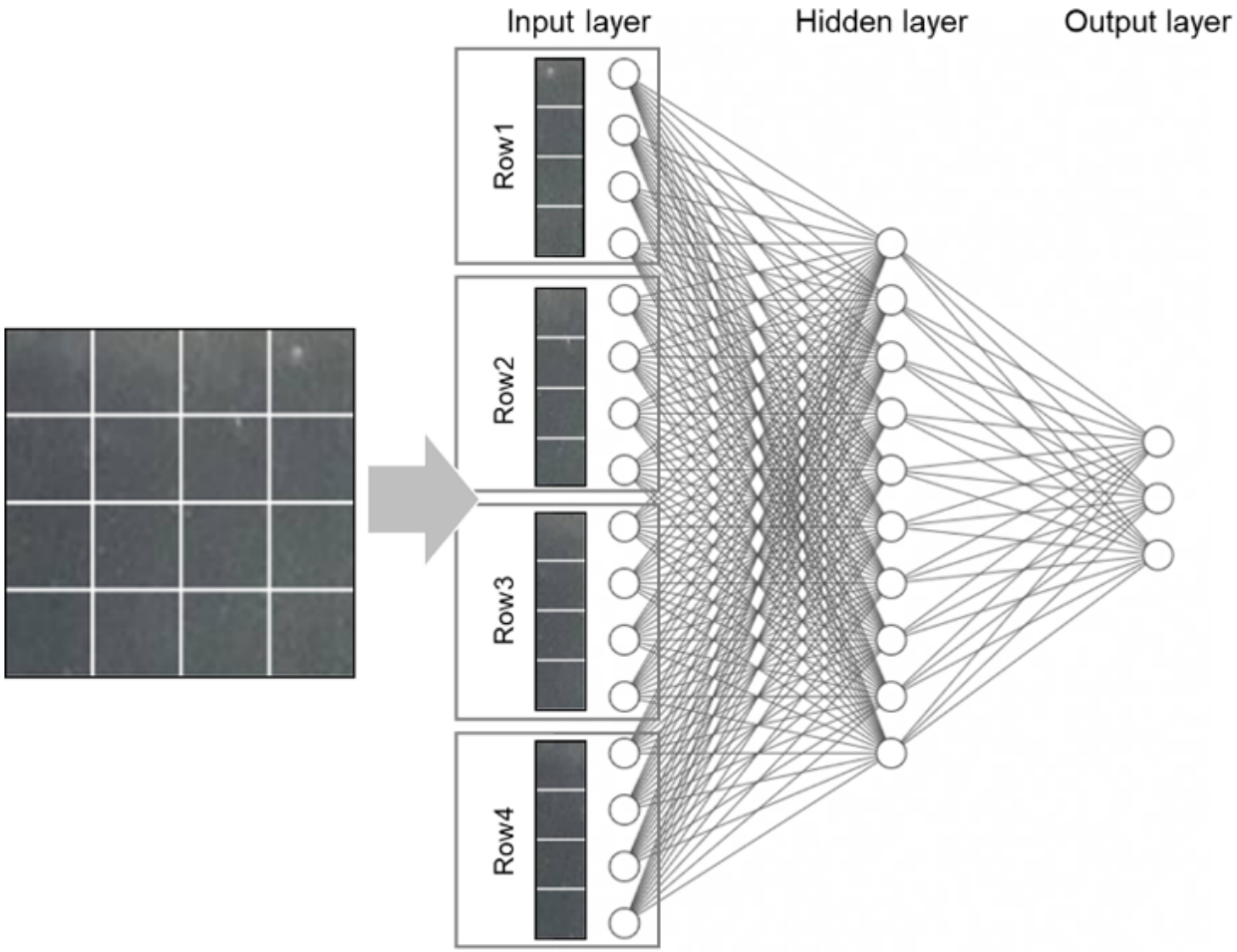

Figure 3

Structure schematic of the fully connected multi-layered neural network.

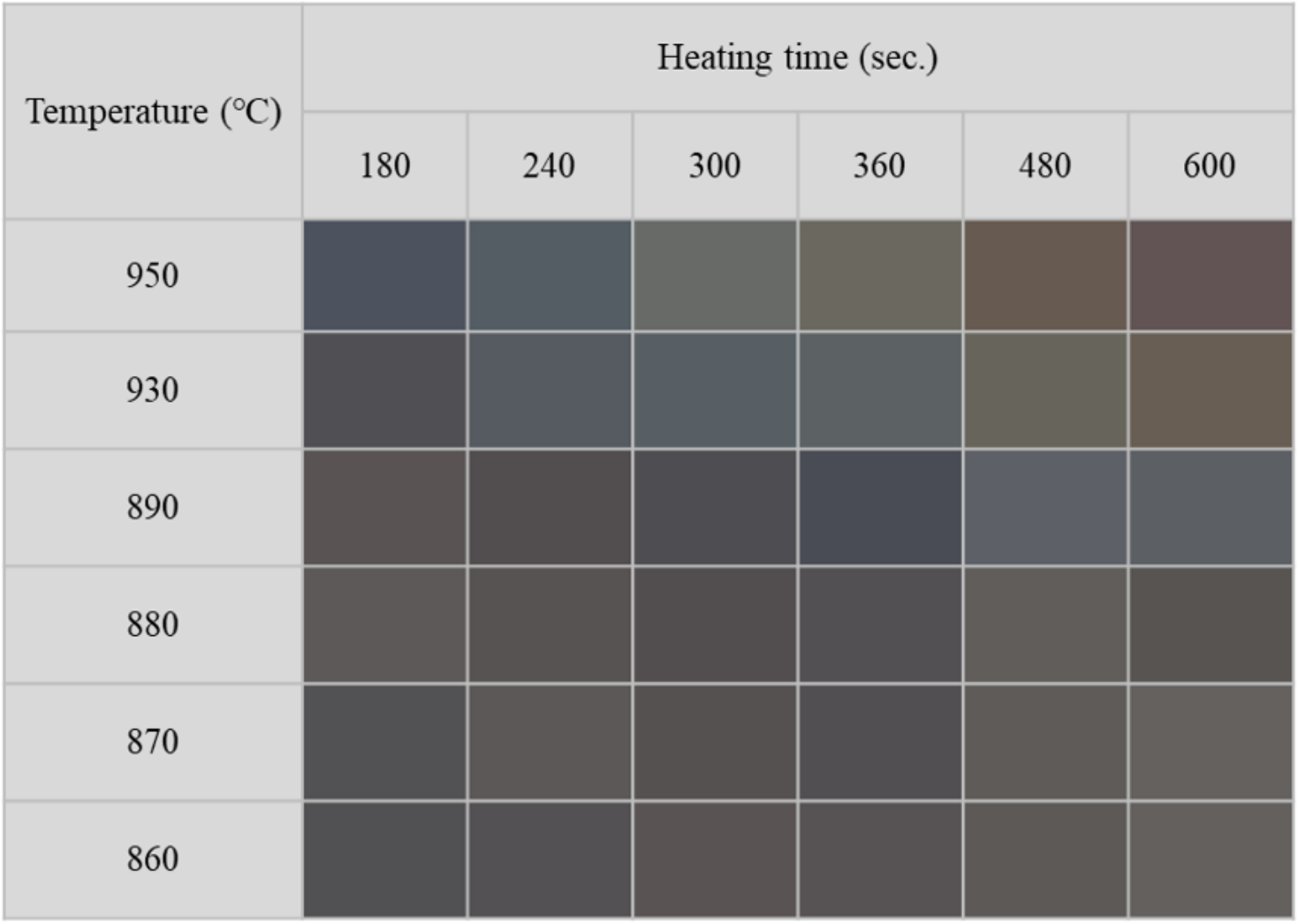

Figure 4

Dataset for training neural network on the hot stamping sheet color.

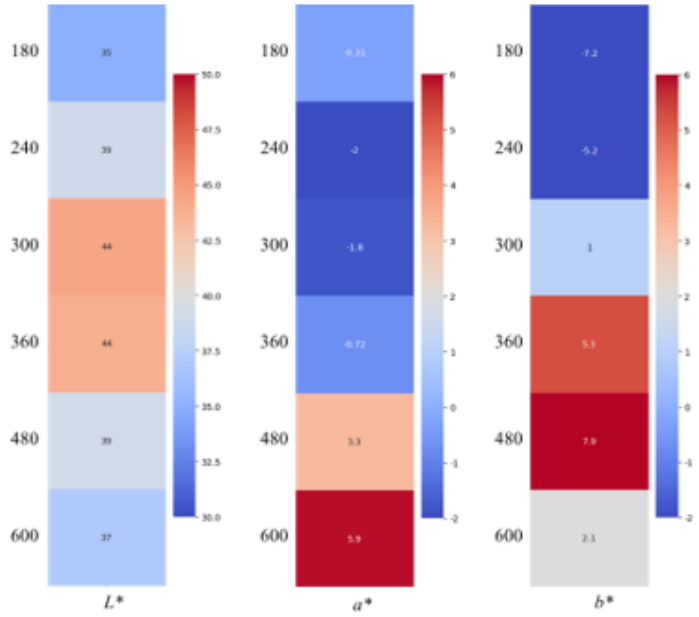

(a) Trend of CIE-Lab coordinate change over heating time (180-600 seconds) at 950 ℃

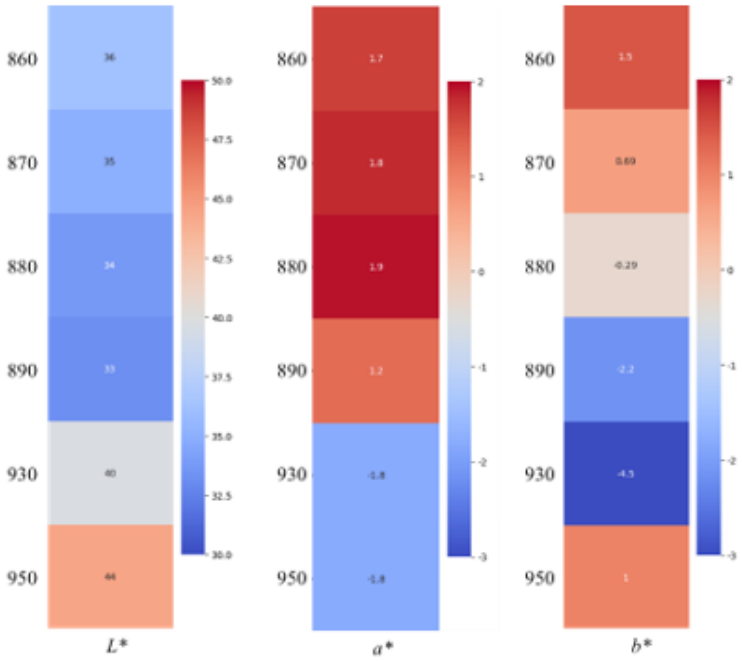

(b) Trend of CIE-Lab coordinate change over heating temperature (860-950 ℃) at 300 seconds

Figure 5

Distribution of hot stamping sheet color according to heating temperature by CIE-Lab coordinate.

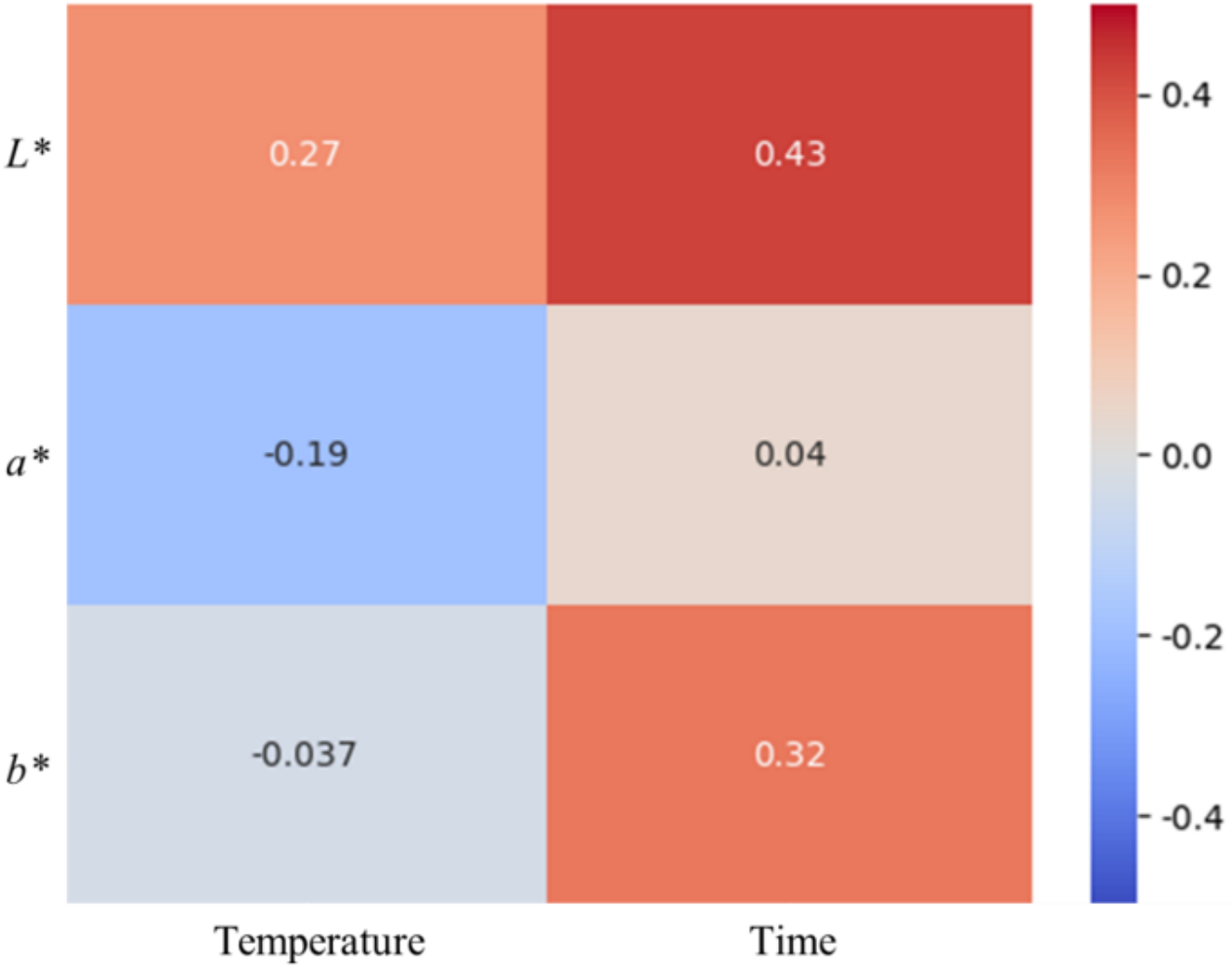

Figure 6

Correlation analysis of hot stamping CIE-Lab coordinate with respect to the heating temperature and time.

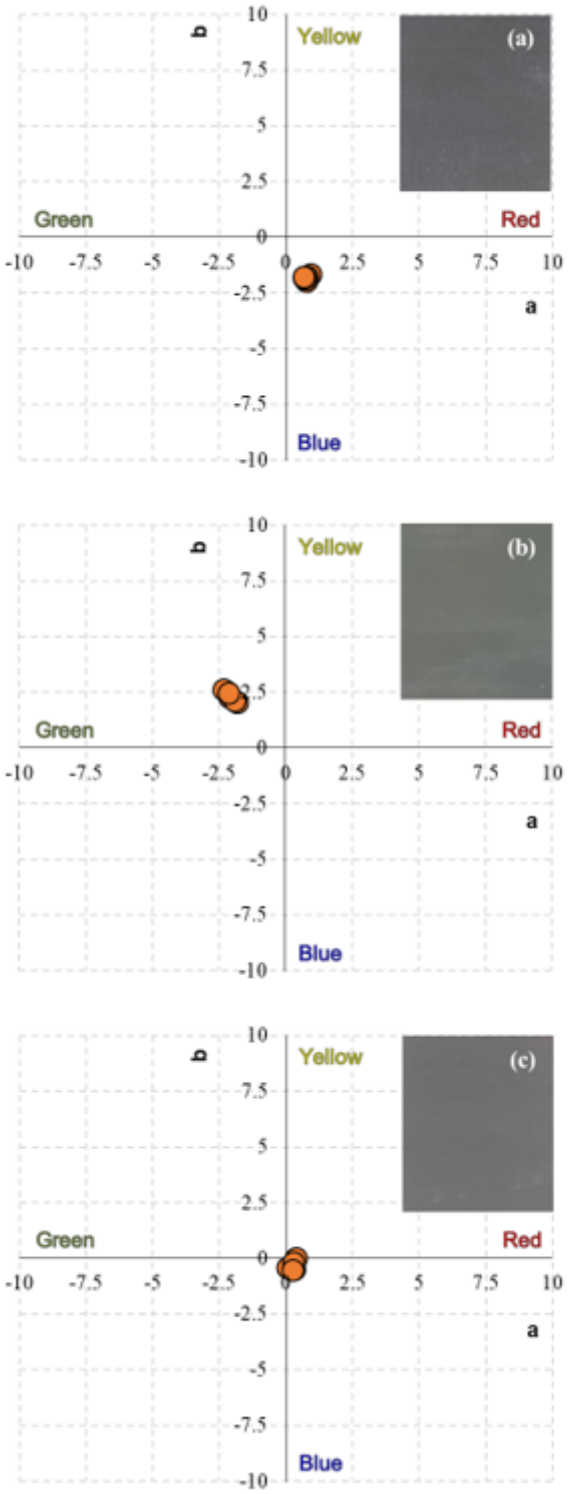

Figure 7

Comparison of image analysis algorithm distribution in different heating conditions.

(a) 880 ℃ for 300 seconds, (b) 930 ℃ for 300 seconds, (c) 960 ℃ for 300 seconds.

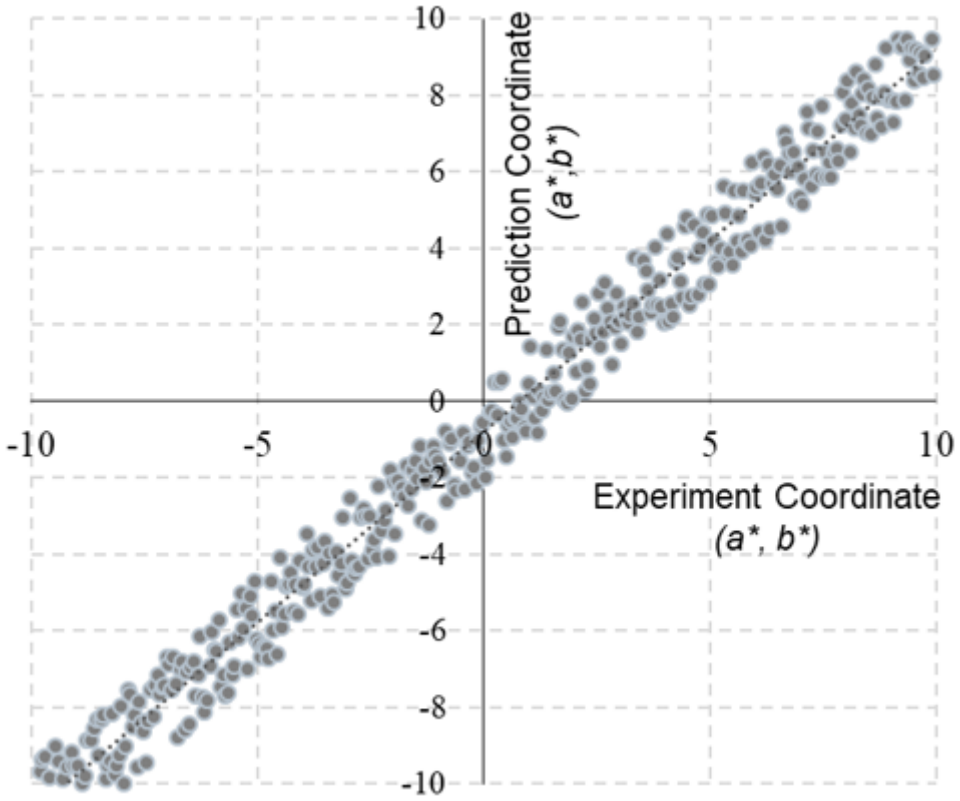

Figure 8

Comparison between the experimental and predicted hot stamping sheet color using the neural network.

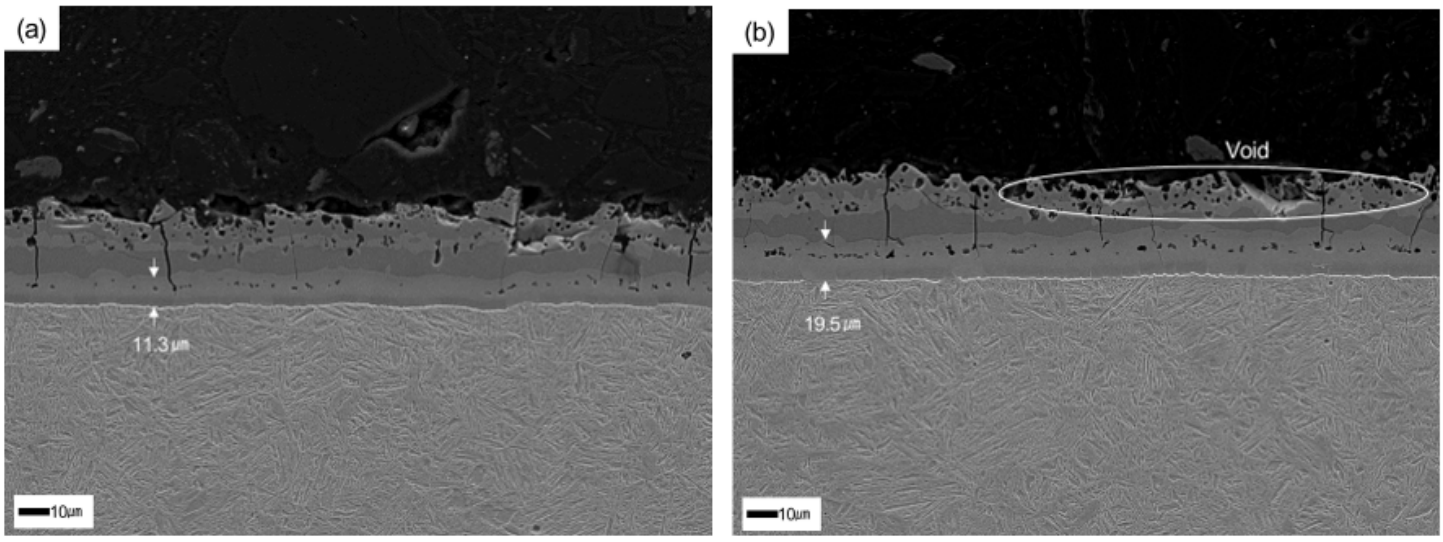

Figure 9

Comparison of inter-diffusion layer thickness in the Al-Si layer under different heating time conditions: (a) 300 seconds at 950 ℃, (b) 600 seconds at 950 ℃.

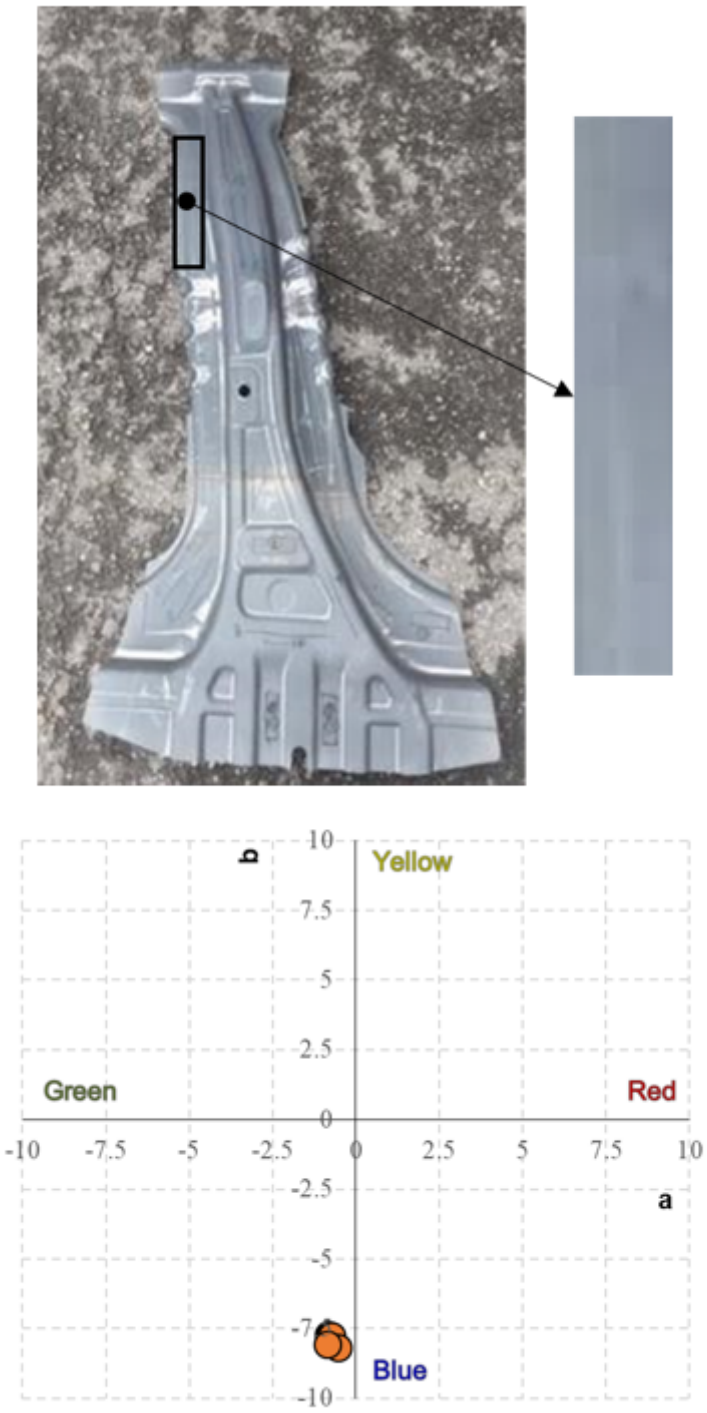

Figure 10

CIE-Lab coordinate analysis at the vehicle part region by neural network for predicting the heating temperature and time.

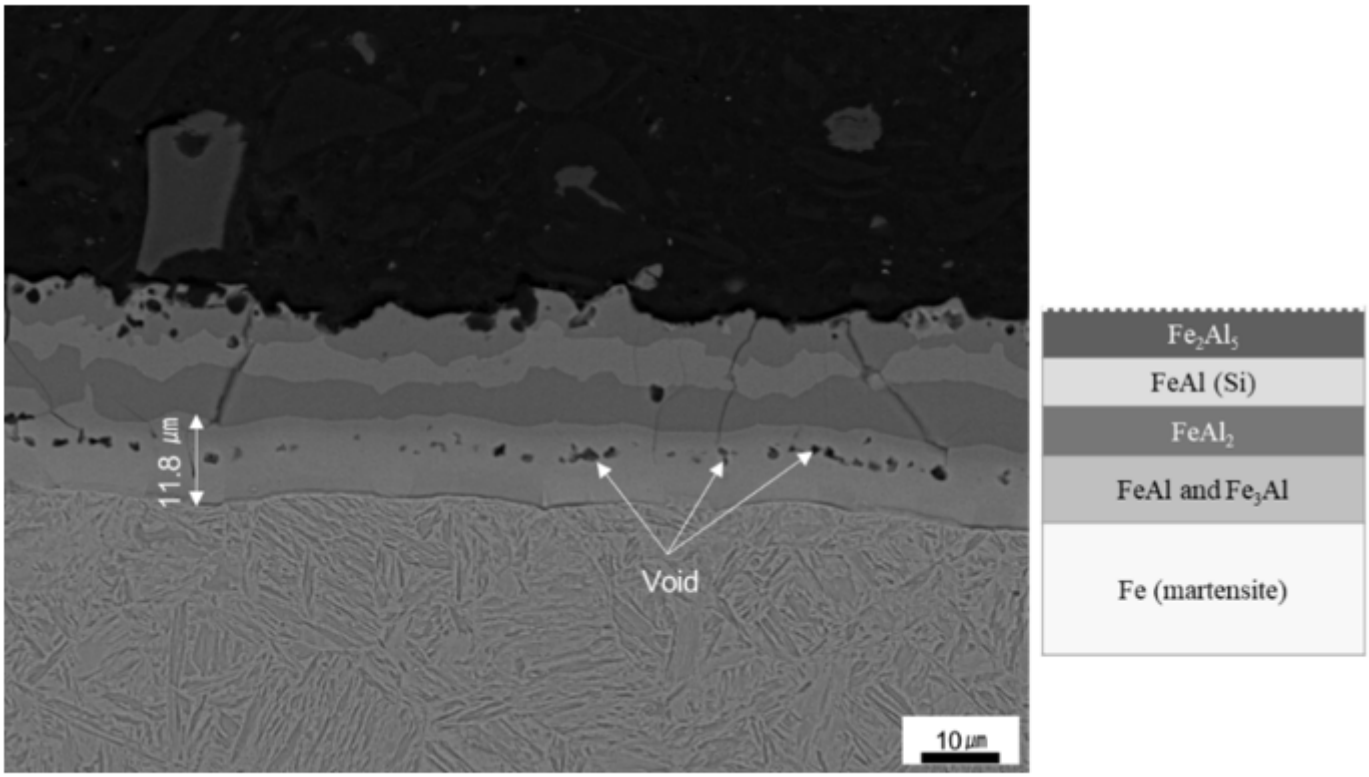

Figure 11

Measured inter-diffusion layer thickness and voids in Al-Si coating 4 layers structure on the vehicle part region [22].

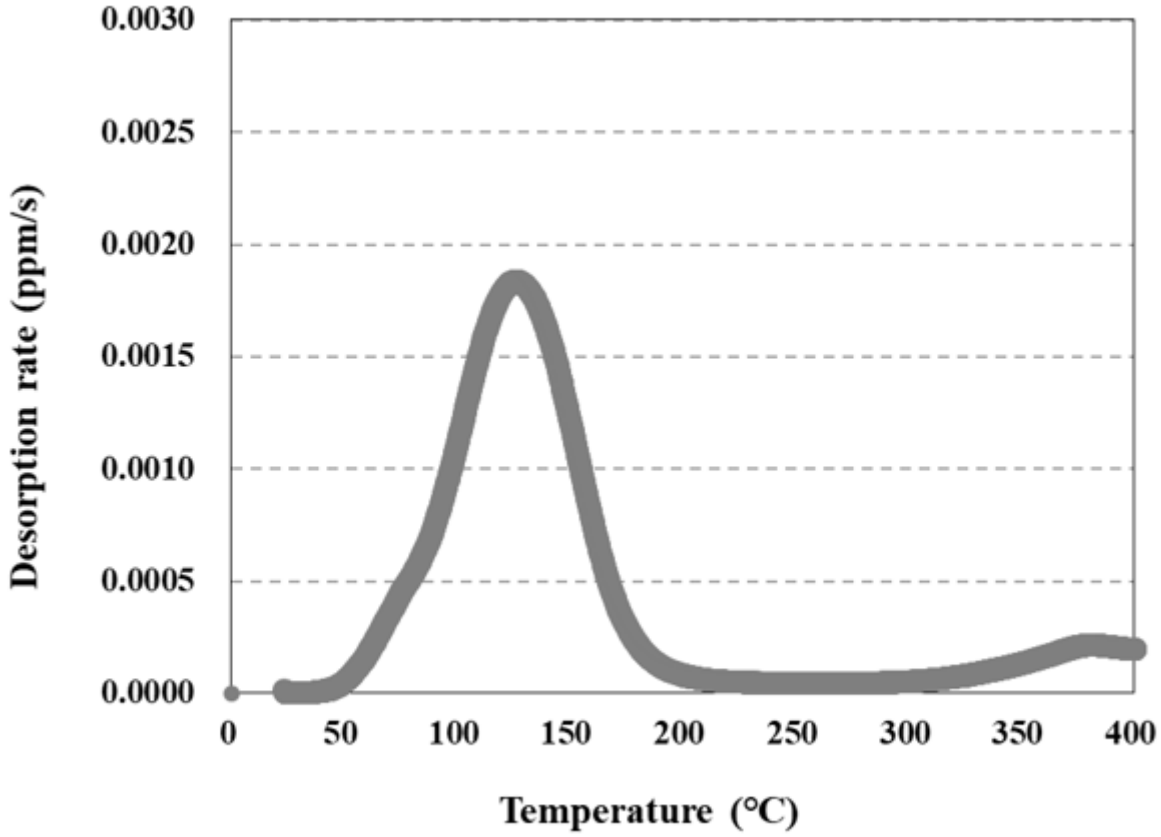

Figure 12

Hydrogen desorption rate as a function of temperature.